Chemical Science

ROYAL SOCIETY OF CHEMISTRY

EDGE ARTICLE

View Article Online
View Journal | View Issue

Cite this: *Chem. Sci.*, 2025, **16**, 20438

All publication charges for this article have been paid for by the Royal Society of Chemistry

Chemoselective cyclodesulfurization *vs.* dehydration enabled by aqueous microdroplet chemistry

Manish Jana, Mousumi Saha and R. Graham Cooks *

Received 24th July 2025
Accepted 29th September 2025

DOI: 10.1039/d5sc05557a

rsc.li/chemical-science

Dehydration reactions are typically favored in microdroplets due to the relatively dry environment at the air–water interface. However, we demonstrate that cyclodesulfurization may outcompete dehydration under these conditions. We report on a catalyst-free method for inducing a two-step cyclodesulfurization in microdroplets under ambient conditions by reacting benzhydrazide with phenyl isothiocyanate. The reaction involves the formation of benzhydrazine-1-carbothioamide, a compound that contains two nucleophilic centers. During competing nucleophilic attacks by hydroxyl and thiol groups, reactive oxygen species at the droplet interface oxidize the thiol, forming the sulfoxylic and then the sulfurous acid. These transient reactive intermediates are detected using online mass spectrometry. The interfacial oxidation reduces thiol nucleophilicity, favoring hydroxyl-mediated nucleophilic attack to form 1,3,4-oxadiazole, a structural motif prevalent in pharmaceuticals. The reaction kinetics are influenced by reagent concentration and the droplet travel distance. The absence of dehydration (commonly found in microdroplet reactions) is a key finding of this work. Our findings also highlight the unique potential of charged microdroplets to promote chemoselective transformations, driven by the distinctive properties of the air–water interface.

Introduction

Microdroplets offer a powerful platform for studying chemical and biological reactions in small volumes, including processes relevant to single cells and even individual molecules.[1–7] Compared to conventional bulk-phase synthesis, microdroplets present a highly distinctive physicochemical environment.[8] Notable phenomena such as accelerated reaction rates, spontaneous redox processes, and the facilitation of otherwise unfavorable reactions have all been observed in microdroplet systems.[9–16] The enhanced reactivity within microdroplets is attributed to a combination of interrelated factors: (a) partial solvation of reactants,[17–20] (b) strong interfacial electric fields,[21,22] (c) ordered molecular orientation at the interface,[23–27] (d) spatial confinement of reagents,[28,29] and (e) localized extremes in pH.[30,31] These factors do not act independently but they contribute synergistically to the unique reactivities observed in microdroplet environments.

Heterocycles serve as a crucial bridge between chemistry and biology, with nitrogen-containing heterocyclic rings found in nearly 75% of small-molecule pharmaceuticals.[32] Due to their widespread biological relevance, these structures are often referred to as "privileged scaffolds".[33] In recent years, a wide array of synthetic strategies—both in conventional bulk chemistry and in microdroplet-based systems—have been developed to construct these valuable frameworks.[34–40] Among these, cyclodesulfurization has gained attention as an efficient method for generating highly substituted heterocycles.[41]

Cyclodesulfurization involves the simultaneous formation of a cyclic structure and the elimination of a sulfur atom from the molecule. Metal-mediated cyclodesulfurization was first introduced in the 1970s.[42]

Since then, a variety of protocols have been tested, most of which rely on metal salts, strong acids, photocatalysts, or combinations thereof—often under elevated temperatures—to drive the reaction.[43–48] These experiments typically also require long reaction times.

Here, we utilize the unique environment of microdroplets to achieve a two-step chemoselective cyclodesulfurization reaction in methanol to produce the 1,3,4-oxadiazole product. Online mass spectrometry was used to monitor the progress of the reaction. Scheme 1 highlights the contrast between traditional, slow, multistep cyclodesulfurization methods and rapid, catalyst-free, chemoselective synthesis enabled by using microdroplets.

Results and discussion

Reactions were performed by electrospraying mixtures of isothiocyanates and benzhydrazide, each 10 mM in reagent-grade methanol (MeOH). Several other solvents (see SI Fig. S1) have

Department of Chemistry, Purdue University, 560 Oval Drive, West Lafayette, Indiana-47907, USA. E-mail: cooks@purdue.edu

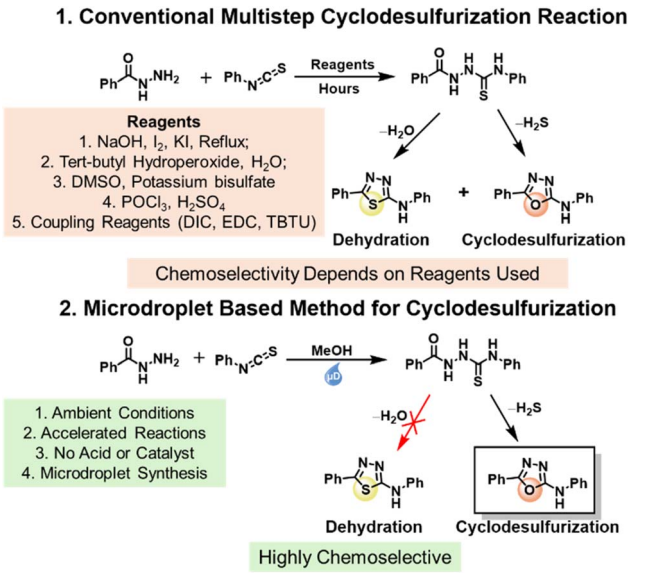

Scheme 1 Comparison of cyclodesulfurization reaction by conventional multistep method *vs.* microdroplet-based method.[41,43–48]

shown similar results provided that water was not rigorously excluded. Electrospraying involved the application of a negative DC potential of −2 kV to a platinum electrode during nano electrospray ionization (nESI) to generate the plume. To investigate the impact of distance on the microdroplet reaction, the distance between the sprayer tip and the mass spectrometer inlet was varied from 3 mm to 120 mm.

Hydrodesulfurization reaction in microdroplets

Fig. 1 presents a detailed overview of the microdroplet-based strategy and the particular reaction studied. An equimolar solution of *p*-nitrophenyl isothiocyanate (**1d**; 10 mM) and benzhydrazide (**2a**; 10 mM) in MeOH was taken up in a nESI capillary, and a spray voltage of −2 kV was applied to generate charged droplets. The ions formed from these droplets were then analyzed using a linear ion trap mass spectrometer. The mass spectrum of the crude reaction mixture recorded in the negative ion mode within milliseconds of initiation exhibits a peak at *m*/*z* 315 corresponding to the formation of benzhydrazine-1-carbothioamide (**3da′**) (Fig. 1b). This molecule has two nucleophilic centers, which can undergo intramolecular reactions to either eliminate water (loss of 18 Da) or hydrogen sulfide (loss of 34 Da), shown in Fig. 2a. It is well known that hydrosulfide is a stronger nucleophile than hydroxide in solution, primarily due to differences in their basicity and polarizability.[49,50] Hydrosulfide has a larger and more polarizable electron cloud as it is less electronegative and larger than oxygen. This allows hydrosulfide to effectively donate electron density to an electrophile, enhancing its nucleophilicity.[51,52]

According to previous literature reports, due to the relatively dry droplet interface, dehydration reactions are often favored in microdroplets.[15,34,35] However, to our surprise, the mass spectrum in the negative ion mode showed a peak at *m*/*z* 281 (Fig. 1b), which corresponds to loss of an H_2S molecule (neutral loss of 34 Da). No peak corresponding to water loss (*m*/*z* 297) was observed in the mass spectrum (Fig. 1b).

To validate the product ion structure as well as to confirm the absence of any non-covalent bond, tandem mass spectrometry was performed for *m*/*z* 315 ([**3da′**-H]$^-$) and 281 ([**3da**-H]$^-$; Fig. 1c and d). The MS/MS spectrum of ion *m*/*z* 315 at a relatively low energy (CID 20) shows neutral loss of 34 Da (*m*/*z* 281, major peak in the mass spectrum) due to loss of H_2S (Fig. 1c). The MS/MS spectra of *m*/*z* 281 in the negative ion mode shows neutral loss of 28 Da due to loss of N_2 (Fig. 1d). The major peak at *m*/*z* 162 corresponds to the cross-ring fragmentation product. The rationalized product ion structures are shown in Fig. 1d.

Conversion ratio determination

Product formation was characterized by the conversion ratio (CR) calculated from the ion intensities of the reactants, intermediates, and products using eqn (1):

$$\text{Conversion ratio (CR)} = \frac{I(\text{P})}{I(\text{P}) + I(\text{R}) + I(\text{INT})} \times 100\% \quad (1)$$

where I(P), I(R), and I(INT) are ion intensities of the products, reactants, and intermediates (respectively) formed during the reaction. CR is a substitute for yield which cannot be measured directly in femtoliter-scale reaction vessels. This point was previously addressed in the SI of our earlier work.[34] Since the ionization efficiencies of the reactants and products may differ, the conversion ratios determined from the mass spectrum may not yield accurate concentrations; however, they can provide an estimate of relative product formation during microdroplet reactions. From the mass spectrum for the above reaction, we found 27% conversion to the oxadiazole product (sprayer to inlet distance of 10 mm).

In the case of microdroplet reactions, the relative product ion intensity should increase with increasing distance between the sprayer and the inlet of the mass spectrometer.[34] Correspondingly, we have observed an increase in ion intensity of the oxadiazole product (increasing the distance from 10 mm to 120 mm) at *m*/*z* of 281 (Fig. 2c and S2), which leads to greater conversion to the product (from 27% to 43%).

Mechanistic investigation into the cyclodesulfurization reaction

Generation of singlet oxygen ($^1O_2$) species through energy transfer at the air–water interface of microdroplets in the absence of light has been reported recently.[53] It is well established that singlet oxygen can oxidize thiols to the corresponding thiosulfinates.[54–59] While investigating the effect of droplet travel distance (inlet of MS to sprayer distance: 3 mm to 120 mm) for this microdroplet reaction using nESI, we detected two new peaks at *m*/*z* of 347 ([**4**-H]$^-$) and 363 ([**5**-H]$^-$) at a distance of ∼120 mm (Fig. 2c and S1). Tandem mass spectrometry (MS/MS) analysis of these ions revealed that both produce a major fragment at *m*/*z* 281, corresponding to the 1,3,4-oxadiazole product (Fig. 2d). These results confirm the presence of transient thiol oxidation intermediates and their

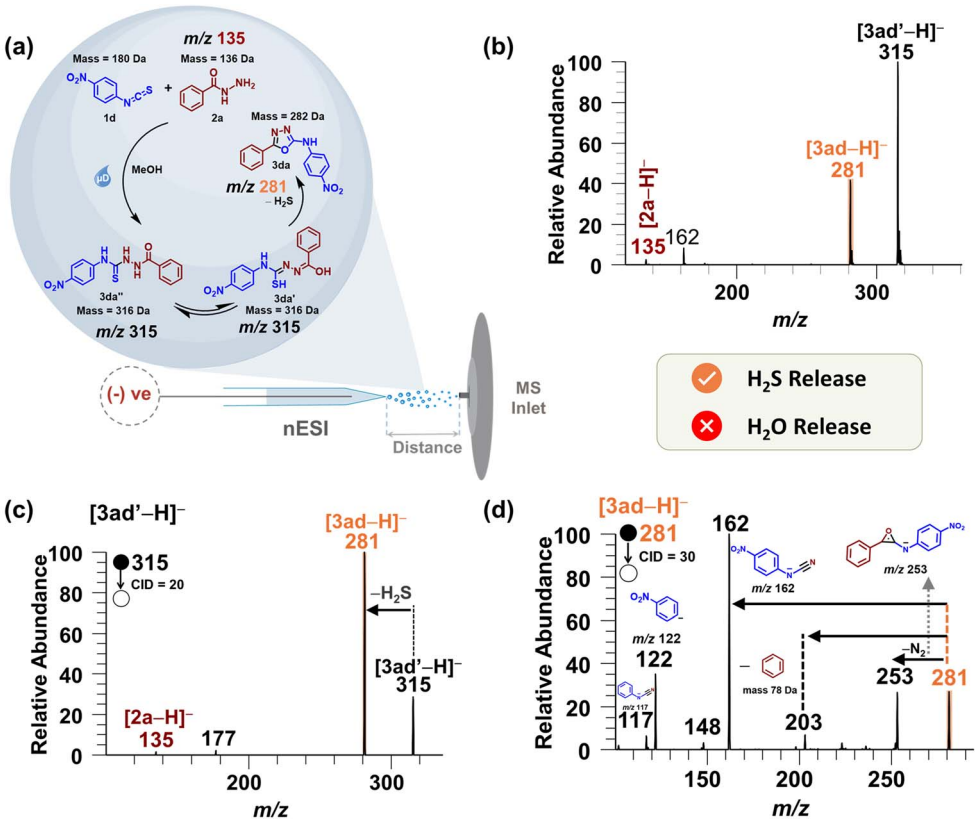

Fig. 1 (a) Cyclodesulfurization reaction between *p*-nitrophenyl isothiocyanate (**1d**) and benzhydrazide (**2a**) in methanol microdroplets. (b) Mass spectrum recorded in negative mode shows peaks for benzhydrazide ([**2a**-H]$^-$; *m*/*z* 135) intermediate ([**3da**'-H]$^-$; *m*/*z* 315) as well as product ([**3da**-H]$^-$; *m*/*z* 281). The orange tick represents the product formed after the release of H_2S. The red cross on water release indicates that no peak corresponding to water loss (*m*/*z* 297) was observed during the reaction. (c) MS/MS spectrum for *m*/*z* 315. (d) MS/MS spectrum for *m*/*z* 281.

conversion to the oxadiazole product during the microdroplet reaction.[12,54–58]

Additionally, 2,2,6,6-tetramethyl-4-piperidone (TEMP) was used to trap the transient sulfur oxidation products. Upon addition of TEMP, the mass spectrum of the reaction mixture reveals a new peak at *m*/*z* 516. MS/MS analysis of this ion yields a product ion at *m*/*z* 281. The mass spectra before and after TEMP addition, along with the corresponding MS/MS spectrum, are presented in the SI, Fig. S3.

At greater sprayer distances, the thiol group undergoes oxidation by reactive oxygen species (ROS) to generate sulfoxide and sulfone. This leads to a reduced nucleophilicity of the thiol, hindering further nucleophilic attack by the thiol group. In the next step, nucleophilic attack by a stronger nucleophile (the hydroxide group) eliminates the thiol group, yielding sulfoxylic acid and sulfurous acid, as shown in Fig. 2b.

When the reaction is conducted using ESSI with nitrogen as the nebulizing gas, the peaks at *m*/*z* 347 and 363 are absent regardless of the sprayer-to-inlet distance (Fig. S4). This suggests that molecular oxygen ($^3O_2$) from ambient air is the reactive oxygen species, and in its excited form, generated at the interface, it yielded the sulfur oxidation products. When performing the reaction using ESSI with oxygen as a nebulizing gas *m*/*z* 281 is the most abundant peak in the mass spectrum (Fig. S5) and as expected the conversion ratio increased significantly from 27% to 49% (at 5 mm sprayer to inlet distance). As suggested by a reviewer, we have also studied the voltage dependence of this reaction using oxygen as a nebulizing gas (Fig. S6); there was no observable dependence.

The distance-dependent behavior indicates that the transformation primarily occurs within the charged microdroplets produced by nESI. As the sprayer distance from the mass spectrometer inlet increases, coulombic explosions and solvent (MeOH) evaporation generate smaller droplets with higher surface-to-volume ratios. The reaction mechanism is unchanged with distance, but the longer interaction times allow the intermediate (thiol group) increased time to react with oxygen, thereby generating more sulfur oxidation side products. The combination of reduced nucleophilicity and extended reaction time accounts for the enhanced product ion intensity observed in the mass spectrum.

Influence of reactant concentration and water content on microdroplet reaction

The concentration of reactants plays an important role in controlling the rate of reactions in microdroplet chemistry. We observed a decrease in conversion ratio when we increased the concentration of both reactants (*p*-nitrophenyl isothiocyanate (**1d**) and benzhydrazide (**2a**)) from 1 mM (CR 32%) to 5 mM (CR

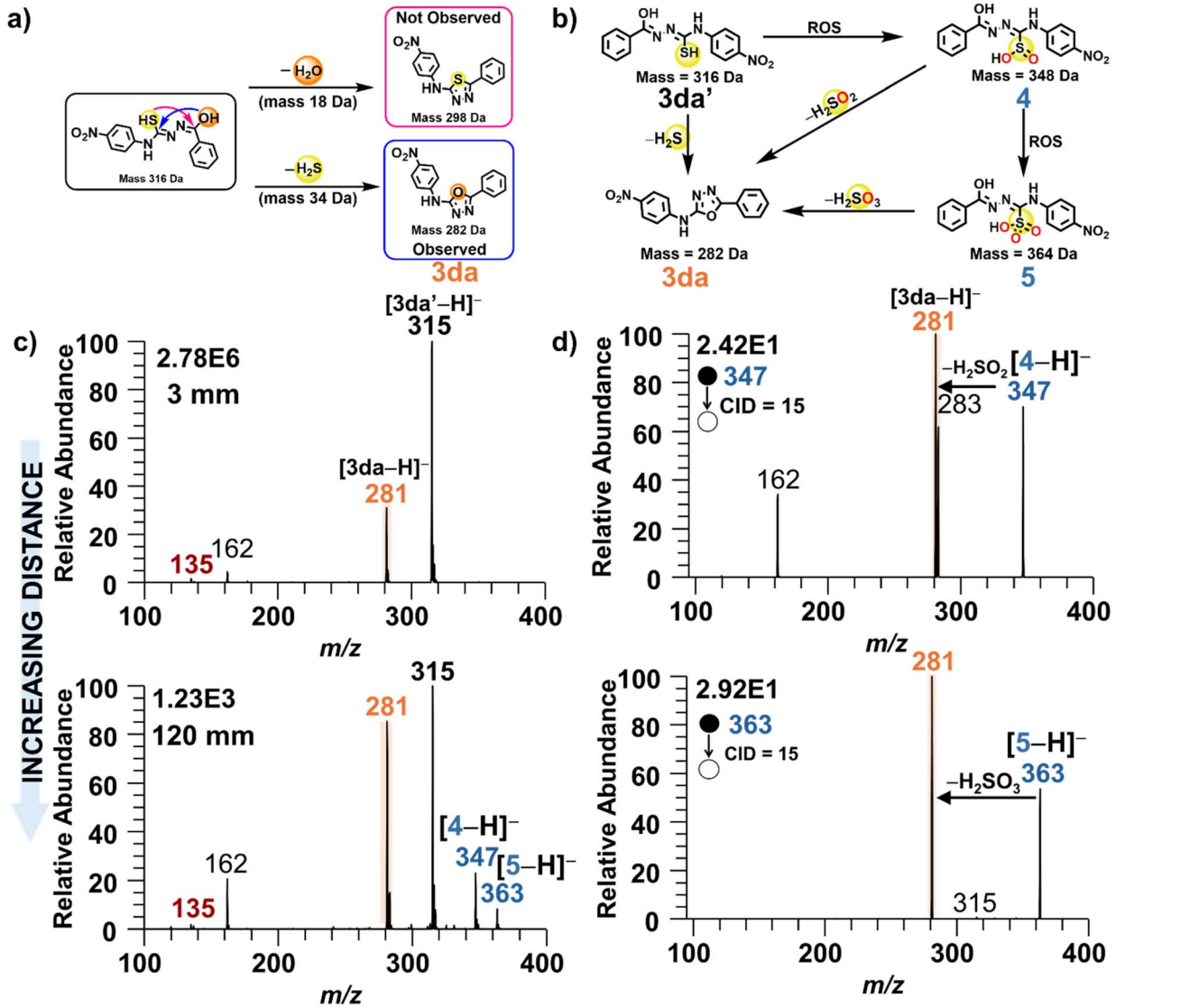

Fig. 2 (a) Different nucleophilic centers in benzhydrazine-1-carbothioamide (**3da'**) that can participate in the formation of cyclic structures. (b) The reaction of the thiol group with reactive oxygen species and (c) the corresponding mass spectra recorded in negative ion mode. With increasing distance of the sprayer to the inlet of the mass spectrometer, two new peaks emerged at *m/z* 347 and *m/z* 363, indicating the formation of a thiol oxidation product. (d) The MS/MS spectra of *m/z* 347 and *m/z* 363.

24%). At lower concentrations, a greater fraction of the reactants are available at the surface of the droplet to participate in the reaction, in contrast to higher concentrations, where a larger proportion of the molecules are at the droplet core and hence unreactive, thus decreasing the overall conversion ratio. Fig. S7a displays a stack of mass spectra at different concentrations. We found that the conversion ratio for product formation falls exponentially with increasing reagent concentration, as shown in Fig. S7b. This exact behavior is not necessarily generalizable to other substrate pairs, as we have not conducted a detailed kinetic analysis of the reaction but the general trend with concentration is known.[21]

In microdroplet reactions, a certain amount of water is essential for generating the highly acidic or basic reagent required to drive acceleration.[36,60,61] During microdroplet formation, methanol tends to evaporate easily due to solvation, enriching the residual droplets in water. To investigate the influence of water content on the reaction, we systematically added varying amounts of water during experiments. Our results show that the highest conversion to the final product was achieved with 2.5% water (conversion ratio, CR ≈ 33%, sprayer to inlet distance 1 cm). However, as the water concentration increased beyond this point, the conversion ratio gradually declined, reaching approximately 27% at 25% water (it's important to note that the methanol used in the reaction inherently contains a small amount of water, which helps to drive the reaction initially without the need for additional water).[62] A plot illustrating the relationship between water content and conversion ratio is provided in the SI, Fig. S8.

Substrate scope

This reaction was also studied in terms of substrate scope using five different isothiocyanates (**1a–1e**) and nine different benzhydrazides (**2a–2i**). An interactive heatmap (Fig. 3) has been generated by using the conversion ratio (CR) for each combination, calculated using eqn (1). Note that the ion intensities were not corrected for competitive fragmentation. The heatmap data suggest that product formation is most favored when electron-donating groups are present in the benzhydrazide and electron-withdrawing groups are present in phenyl isothiocyanate. The mass spectra for all the substrates, corresponding MS/MS spectra and the Hammett plots are given in the SI, Fig. S10–S58.

Scale up for further characterization using NMR

For characterization by ^{1}H NMR, the reaction was scaled up using a single sprayer. Instead of combining the reagents in one syringe, each reagent was loaded into separate syringes. The reagents briefly mix for a few milliseconds at a T-junction just prior to spraying. A schematic diagram of the scale-up setup is provided in the SI, Fig. S9. The reaction gave a relatively clean conversion to the 1,3,4-oxadiazole product (higher yield) when the reagent concentrations are 50 mM each in methanol (final concentration 25 mM) and are sprayed at a rate of 50 μL min^{-1}.

The collected products were directly dissolved in deuterated solvents for NMR characterization, without any workup or purification. This highlights a key advantage of microdroplet chemistry, and the gentle methods used relative to conventional synthetic methods. A representative ^{1}H NMR spectrum obtained from the reaction between *p*-methyl phenyl isothiocyanate (**1b**; 50 mM in 5 mL MeOH) and benzhydrazide (**2a**; 50 mM in 5 mL MeOH), using a single sprayer and recorded in DMSO-d$_6$, is shown in Fig. 4. After 3 h of spraying, 47 mg of the oxadiazole product was isolated, equivalent to an yield of 75%. The peaks corresponding to the protons of the intermediate benzhydrazine-1-carbothioamide were also observed in the ^{1}H NMR. Note that no chromatographic separations were performed to purify the product before NMR analysis. We suggest that the rate of product formation can be significantly improved by using multiple sprayers as well as a solvent recycling system.[63–65] ^{1}H NMR spectra for additional oxadiazole products are provided in the SI, Fig. S21, S31, S40, and S47. In all cases, the yields were greater than 60% as determined from the NMR spectra.

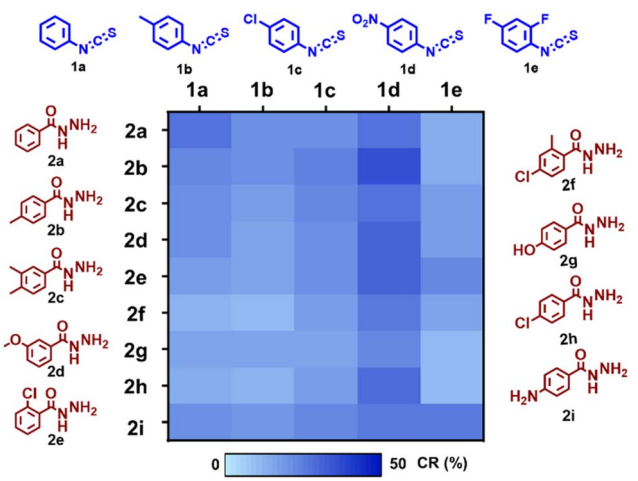

Fig. 3 Heatmap showing the cyclodesulfurization reaction outcomes using various isothiocyanates (**1a–1e**) and benzhydrazides (**2a–2i**) in methanol, with manual preparation of reaction mixtures and analysis by nESI (distance was kept at 1 cm and total concentration 5 mM). The heatmap is based on conversion ratios (CR) calculated from uncorrected ion intensities.

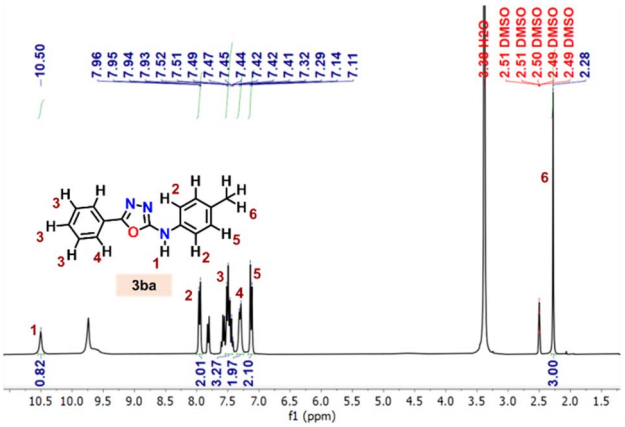

Fig. 4 ^{1}H NMR spectrum for the microdroplet reaction between *p*-methyl phenyl isothiocyanate (**1b**) and benzhydrazide (**2a**) in DMSO-d$_6$ (300 MHz).

Conclusions

Although hydrosulfide is widely recognized as a stronger nucleophile than hydroxide, our results show that in charged microdroplets, the desulfurization reaction is favored over dehydration, enabling the efficient formation of 1,3,4-oxadiazole molecules. The reaction proceeds with high chemoselectivity and at a significantly accelerated rate compared to bulk-phase conditions, without the need for a catalyst. During competing nucleophilic attacks by hydroxyl and thiol groups, reactive oxygen species (ROS) at the droplet interface oxidize the thiol, forming sulfoxylic acid and sulfurous acid. This oxidation reduces the nucleophilicity of the thiol, thereby favoring hydroxyl-mediated nucleophilic attack. The dependence of reaction on concentration suggests that at lower concentration, most of the reactants are available at the surface of the droplet to participate in the reaction, in contrast to the high concentration, where molecules at the droplet core are unreactive, thus decreasing the overall conversion ratio. The reaction's substrate scope was investigated, and scaled up to milligram quantities using a single-sprayer setup, for characterization by NMR.

Author contributions

R. G. Cooks, M. Jana, and M. Saha designed the experiments. M. Jana and M. Saha performed the experiments. R. G. Cooks, M.

Jana, and M. Saha analyzed the results and wrote the manuscript.

Conflicts of interest

There are no conflicts to declare.

Data availability

All data on which this publication is based appear either in the main text or in the supplementary information (SI). The underlying raw data are available on request to the authors. Supplementary information: general information, scale up experimental details, mass spectrum and MS/MS data for all substrates. See DOI: https://doi.org/10.1039/d5sc05557a.

Acknowledgements

We acknowledge the financial support from the Multi-University Research Initiative of the Air Force Office of Scientific Research (FA9550-21-1-0170) *via* Stanford University (subaward 62741613-204669) and NSF Center for Bioanalytic Metrology (supported by the National Science Foundation under grant IIP-307915PU) for providing funding for this project. M. S. acknowledges support from the American Chemical Society Division of Analytical Chemistry Graduate Fellowship sponsored by Eli Lilly and Co.

References

1 M. Girod, E. Moyano, D. I. Campbell and R. G. Cooks, *Chem. Sci.*, 2011, **2**, 501–510.
2 B. K. Spoorthi, K. Debnath, P. Basuri, A. Nagar, U. V. Waghmare and T. Pradeep, *Science*, 2024, **384**, 1012–1017.
3 X. Zhong, H. Chen and R. N. Zare, *Nat. Commun.*, 2020, **11**, 1049.
4 I. Nam, J. K. Lee, H. G. Nam and R. N. Zare, *Proc. Natl. Acad. Sci. U. S. A.*, 2017, **114**, 12396–12400.
5 X. Song, C. Basheer and R. N. Zare, *Proc. Natl. Acad. Sci. U. S. A.*, 2023, **120**, e2301206120.
6 S. Banerjee and R. N. Zare, *Angew. Chem., Int. Ed.*, 2015, **54**, 14795–14799.
7 J. K. Lee, D. Samanta, H. G. Nam and R. N. Zare, *Nat. Commun.*, 2018, **9**, 1562.
8 X. Yan, R. M. Bain and R. G. Cooks, *Angew. Chem., Int. Ed.*, 2016, **55**, 12960–12972.
9 L. Qiu and R. G. Cooks, *Angew. Chem., Int. Ed.*, 2022, **61**, e202210765.
10 L. Qiu and R. G. Cooks, *Angew. Chem., Int. Ed.*, 2024, **63**, e202400118.
11 J. K. Lee, D. Samanta, H. G. Nam and R. N. Zare, *J. Am. Chem. Soc.*, 2019, **141**, 10585–10589.
12 L. Qiu, M. D. Psimos and R. G. Cooks, *J. Am. Soc. Mass Spectrom.*, 2022, **33**, 1362–1367.
13 S. Jin, H. Chen, X. Yuan, D. Xing, R. Wang, L. Zhao, D. Zhang, C. Gong, C. Zhu, X. Gao, Y. Chen and X. Zhang, *JACS Au*, 2023, **3**, 1563–1571.
14 A. Nandy, A. Rana, N. Shibata and S. Banerjee, *J. Am. Chem. Soc.*, 2025, **147**, 22542–22549.
15 D. T. Holden, N. M. Morato and R. G. Cooks, *Proc. Natl. Acad. Sci. U. S. A.*, 2022, **119**, e2212642119.
16 E. Gnanamani, X. Yan and R. N. Zare, *Angew. Chem., Int. Ed.*, 2020, **59**, 3069–3072.
17 C. Zhu, L. N. Pham, X. Yuan, H. Ouyang, M. L. Coote and X. Zhang, *J. Am. Chem. Soc.*, 2023, **145**, 21207–21212.
18 A. Nandy, A. Kumar, S. Mondal, D. Koner and S. Banerjee, *J. Am. Chem. Soc.*, 2023, **145**, 15674–15679.
19 B. Gong, D. Li, X. Li, D. Zhang, D. Xing, L. Zhao, X. Yuan and X. Zhang, *J. Am. Chem. Soc.*, 2022, **144**, 3510–3516.
20 (*a*) A. Kumar, S. Mondal and S. Banerjee, *J. Am. Chem. Soc.*, 2021, **143**, 2459–2463; (*b*) A. Kumar, S. Mondal, M. Mofidfar, R. N. Zare and S. Banerjee, *J. Am. Chem. Soc.*, 2022, **144**, 7573–7577; (*c*) S. Banerjee, *Int. J. Mass Spectrom.*, 2023, **486**, 117024.
21 L. Qiu, Z. Wei, H. Nie and R. G. Cooks, *ChemPlusChem*, 2021, **86**, 1362–1365.
22 K. D. Judd, S. W. Parsons, D. B. Eremin, V. V. Fokin and J. M. Dawlaty, *Chem. Sci.*, 2024, **15**, 8346–8354.
23 Z. Song, C. Liang, K. Gong, S. Zhao, X. Yuan, X. Zhang and J. Xie, *J. Am. Chem. Soc.*, 2023, **145**, 26003–26008.
24 C. F. Chamberlayne and R. N. Zare, *J. Chem. Phys.*, 2020, **152**, 184702.
25 H. Xiong, J. K. Lee, R. N. Zare and W. Min, *J. Phys. Chem. Lett.*, 2020, **11**, 7423–7428.
26 H. Hao, I. Leven and T. Head-Gordon, *Nat. Commun.*, 2022, **13**, 280.
27 R. A. LaCour, J. P. Heindel, R. Zhao and T. Head-Gordon, *J. Am. Chem. Soc.*, 2025, **147**, 6299–6317.
28 C. Feng and L. Zhang, *Mater. Horiz.*, 2024, **11**, 1515–1527.
29 K. Gong, A. Nandy, Z. Song, Q.-S. Li, A. Hassanali, G. Cassone, S. Banerjee and J. Xie, *J. Am. Chem. Soc.*, 2024, **146**, 31585–31596.
30 A. J. Colussi, S. Enami and S. Ishizuka, *ACS Earth Space Chem.*, 2021, **5**, 2341–2346.
31 M. Li, Y. Kan, H. Su, U. Pöschl, S. H. Parekh, M. Bonn and Y. Cheng, *Chem*, 2023, **9**, 1036–1046.
32 C. M. Marshall, J. G. Federice, C. N. Bell, P. B. Cox and J. T. Njardarson, *J. Med. Chem.*, 2024, **67**, 11622–11655.
33 M. E. Welsch, S. A. Snyder and B. R. Stockwell, *Curr. Opin. Chem. Biol.*, 2010, **14**, 347–361.
34 M. Jana, K. Unni, T. Pradeep and R. G. Cooks, *ACS Sustain. Chem. Eng.*, 2025, **13**, 7645–7654.
35 J. Ghosh and R. G. Cooks, *Chem. Sci.*, 2025, **16**, 8800–8806.
36 J. Li, J. Sun, Y. Wang, J. Liu and H. Cheng, *ACS Sustain.Chem. Eng.*, 2025, **13**, 571–582.
37 D. B. Eremin and V. V. Fokin, *J. Am. Chem. Soc.*, 2021, **143**, 18374–18379.
38 C. Dai, C. Huang, M. Ye, J. Liu and H. Cheng, *J. Org. Chem.*, 2024, **89**, 14818–14830.

39 N. Sahota, D. I. AbuSalim, M. L. Wang, C. J. Brown, Z. Zhang, T. J. El-Baba, S. P. Cook and D. E. Clemmer, *Chem. Sci.*, 2019, **10**, 4822–4827.
40 D. Kuai, H. Cheng, K.-Y. Kuan and X. Yan, *Chem. Commun.*, 2021, **57**, 3757–3760.
41 T. Rerkrachaneekorn, R. M. Annuur, S. Pornsuwan, M. Sukwattanasinitt and S. Wacharasindhu, *Sci. Rep.*, 2025, **15**, 4096.
42 G. C. Vogel and R. S. Drago, *J. Am. Chem. Soc.*, 1970, **92**, 5347–5351.
43 S.-J. Yang, S.-H. Lee, H.-J. Kwak and Y.-D. Gong, *J. Org. Chem.*, 2013, **78**, 438–444.
44 D. Kumar Sigalapalli, M. Kadagathur, A. Sujat Shaikh, G. S. Jadhav, B. Bakchi, B. Nagendra Babu and N. D. Tangellamudi, *ChemistrySelect*, 2020, **5**, 13248–13258.
45 P. A. Yakkala, I. A. Khan, S. R. Dannarm, J. Aboti, R. Sonti, S. Shafi and A. Kamal, *J. Org. Chem.*, 2023, **88**, 12216–12223.
46 T. Fang, Q. Tan, Z. Ding, B. Liu and B. Xu, *Org. Lett.*, 2014, **16**, 2342–2345.
47 M. Sciarretta, M. Barawi, C. Navío, V. A. P. O. Shea, M. Blanco and J. Alemán, *ACS Appl. Mater. Interfaces*, 2022, **14**, 34975–34984.
48 F. Golmohammadi, S. Balalaie, F. Hamdan and S. Maghari, *New J. Chem.*, 2018, **42**, 4344–4351.
49 E. P. L. Hunter and S. G. Lias, *J. Phys. Chem. Ref. Data*, 1998, **27**, 413–656.
50 J. E. Bartmess, J. A. Scott and R. T. McIver Jr, *J. Am. Chem. Soc.*, 1979, **101**, 6046–6056.
51 D. J. Defrees and A. D. McLean, *J. Comput. Chem.*, 1986, **7**, 321–333.
52 Z. B. Maksić, B. Kovačević and R. Vianello, *Chem. Rev.*, 2012, **112**, 5240–5270.
53 F. Li, J. Lv, A. He, J. Xu, L. Zhao, X. Wang, L. Mao, S. Li, H. Wang, Y. Wang and G. Jiang, *J. Am. Chem. Soc.*, 2025, **147**, 30574–30581.
54 Z. Rao, X. Li, Y.-G. Fang, J. S. Francisco, C. Zhu and C. Chu, *J. Am. Chem. Soc.*, 2023, **145**, 10839–10846.
55 D. D. Saraev and D. A. Pratt, *Chem. Sci.*, 2024, **15**, 20421–20432.
56 W. Wang, Y. Liu, T. Wang, Q. Ge, K. Li, J. Liu, W. You, L. Wang, L. Xie, H. Fu, J. Chen and L. Zhang, *J. Am. Chem. Soc.*, 2024, **146**, 6580–6590.
57 D. Schilter, *Nat. Rev. Chem.*, 2017, **1**, 0013.
58 A. Asserghine, A. Baby, J. N'Diaye, A. I. B. Romo, S. Das, C. A. Litts, P. K. Jain and J. Rodríguez-López, *J. Am. Chem. Soc.*, 2025, **147**, 11851–11858.
59 J. Sun, X. Ge, Y. Gao, M. Zhang, Q. Zhao, G. Hou, X. Wang, Y. Yin, J. Ouyang and N. Na, *Chem. Sci.*, 2024, **15**, 16724–16732.
60 Z. Song, C. Zhu, K. Gong, R. Wang, J. Zhang, S. Zhao, Z. Li, X. Zhang and J. Xie, *J. Am. Chem. Soc.*, 2024, **146**, 10963–10972.
61 M.-Y. Jia, Y.-W. Zhou, J.-L. Yang, Q. Liu and Z.-F. Cai, *Nat. Commun.*, 2025, **16**, 7453.
62 L. Qiu, M. Saha, S. Kraft, E. T. Dziekonski, C. J. Welch, Y. Dai, A. Kaerner and R. G. Cooks, *Angew. Chem., Int. Ed.*, 2023, **62**, e202310884.
63 T. Müller, A. Badu-Tawiah and R. G. Cooks, *Angew. Chem., Int. Ed.*, 2012, **51**, 11832–11835.
64 X. Yan, H. Cheng and R. N. Zare, *Angew. Chem., Int. Ed.*, 2017, **56**, 3562–3565.
65 H. Nie, Z. Wei, L. Qiu, X. Chen, D. T. Holden and R. G. Cooks, *Chem. Sci.*, 2020, **11**, 2356–2361.